Beamforming-based Conformal Patch Antenna Array Design for Enhanced Community Cellular Coverage

Joaquin M. Menguito
Electrical and Electronics Engineering Institute
University of the Philippines Diliman College of Engineering
Quezon City, Philippines
joaquin.menguito@eee.upd.edu.ph

Ryan Jacob H. Tanco
Electrical and Electronics Engineering Institute
University of the Philippines Diliman College of Engineering
Quezon City, Philippines
ryan.jacob.tanco@eee.upd.edu.ph

Paul Jason R. Co
Electrical and Electronics Engineering Institute
University of the Philippines Diliman College of Engineering
Quezon City, Philippines
paul.co@eee.upd.edu.ph

Philip A. Martinez
Electrical and Electronics Engineering Institute
University of the Philippines Diliman College of Engineering
Quezon City, Philippines
philip.martinez@eee.upd.edu.ph

***Abstract*—A beamforming-based conformal 4-element patch antenna array was designed to address coverage gaps in directional antennas used for rural GSM applications. Operating at 900 MHz, the system integrates a Butler matrix for fixed-angle beam steering and employs inset-fed microstrip patch antennas on a flexible polyimide substrate. Various curvatures were tested, and the 180° curved configuration achieved the best performance. It produced main lobes at -23.0°, 44.0°, 18.0°, and -65.0° relative to broadside, with realized gains of around 3-4 dBi and 3 dB beamwidths of around 30-50° — demonstrating promising applicability for enhancing coverage in community cellular deployments.**

***Index Terms*—Beamforming, Conformal Antenna Array, Butler Matrix, Rural Cellular Coverage, Patch Antenna**

I. Introduction & Project Overview

In the Philippines, many rural areas still lack reliable cellular coverage despite advances in wireless technology. This issue comes from the country's complex geography, low population densities, and high infrastructure costs in remote regions [1]. While urban areas transition to 4G and 5G networks [2], rural communities remain dependent on outdated systems or have no connectivity at all. This digital divide limits access to services such as communication, education, and emergency response.

Several efforts have aimed to improve rural connectivity using cost-effective technologies. A notable initiative is the Village Base Station (VBTS) project launched in 2017 [3], which enabled community-owned GSM networks using low-cost, solar-powered, and software-defined base stations. In the systems of the VBTS project, antennas are critical for signal transmission and reception. However, the directional antennas used operated only at the quadrantal angles — with gains of approximately 3.5 dBi (0°), 3 dBi (90°), 4 dBi (180°), and 1.5 dBi (270°) — resulting in coverage gaps between beams [4].

To address these limitations, beamforming with a Butler matrix — a passive network that distributes signal amplitude and phase — allows fixed-angle steering when feeding a patch antenna array. While this avoids active components, it is typically used in high-frequency planar systems, making adaptation to low-frequency GSM networks less common. For instance, Yusnita et al. [5] and Tseng et al. [6] developed Butler matrix-based systems at 38 GHz and 60 GHz, respectively, which require precise fabrication and are unsuitable for low-cost GSM deployment.

The directional antennas in [4] created blind spots between directional lobes. To enhance spatial coverage, this study proposes a Butler matrix-fed patch antenna array. Conventional arrays, however, steer beams at fixed angles (typically $\pm 14.5°$ and $\pm 48.6°$), which may not provide full area coverage. Hence, this design modifies the array's geometry to broaden angular range while maintaining acceptable gain — improving the VBTS project's reliability by reducing coverage gaps.

An antenna for wide-area cellular coverage was designed using CST Studio Suite and MATLAB. A patch antenna operating at 900 MHz was integrated into a 4-element array fed by a Butler matrix at the same frequency. The array was curved to optimize coverage and maintain reasonable gain, with tuning to refine performance. TAlthough telecommunication companies are now pushing for 4G and 5G in these areas, the 900 MHz band remains relevant as it can also be used for 4G LTE Band 8 and 5G New Radio Band n8 — ensuring the antenna supports both current and future rural wireless communication needs.

II. 4×4 Butler Matrix

One of the three main components of the Butler matrix is the 90° hybrid coupler. In designing this hybrid coupler, the

979-8-3315-6946-4/25/$31.00

width of the microstrips can be obtained with the equation from [7]:

$$W = \frac{W}{h} \cdot h = \frac{8 \cdot \exp(h')}{\exp(2 \cdot h') - 2} \cdot h$$

where $h' = \left(\frac{Z_0}{60}\right) \cdot \sqrt{\frac{\epsilon_r+1}{2}} + \left(\frac{\epsilon_r-1}{\epsilon_r+1}\right) \cdot \left(0.226 + \frac{0.120}{\epsilon_r}\right)$. The physical lengths of the microstrips can be calculated by:

$$L = \frac{L_e}{2\pi} \cdot \lambda_g$$

Where the electrical length, L_e, is set to $\frac{\pi}{4}$ (90°). Table I presents the dimensions of the 90° hybrid coupler:

TABLE I: Initial Dimensions of the 90° Hybrid Coupler

Parameter	$Z_0 = 50\,\Omega$	$Z_0 = \frac{50}{\sqrt{2}}\,\Omega$
Length (mm)	50.27	49.26
Width (mm)	3.39	5.68

Another component of the matrix is the crossover, which is used to mitigate signal interference at physical intersections by using two cascaded 90° hybrid couplers to isolate and recombine signals along their intended paths.

Lastly, a component of the matrix known as the 45° phase shifter introduces a shift in the phase when a certain change in the length by ΔL [8], which can be obtained by the equation $\Delta L = \frac{\theta \cdot \lambda_g}{360°}$, where θ is the desired phase shift (45°), and λ_g is the guided wavelength. Substituting the values, ΔL is obtained as 25.1375 mm. Given this shifter length, the width is initially set to be the same as the length. It is worth noting that the length is expected to change upon integration and tuning.

A. Final Butler Matrix Design

The Butler matrix was integrated step-by-step, simulating and examining the phase differences at each level through a bottom-up approach — from the input to the output ports — to validate functionality. Likewise, an iterative approach was used to adjust the 0° and 45° phase shifters to produce the required phase differences.

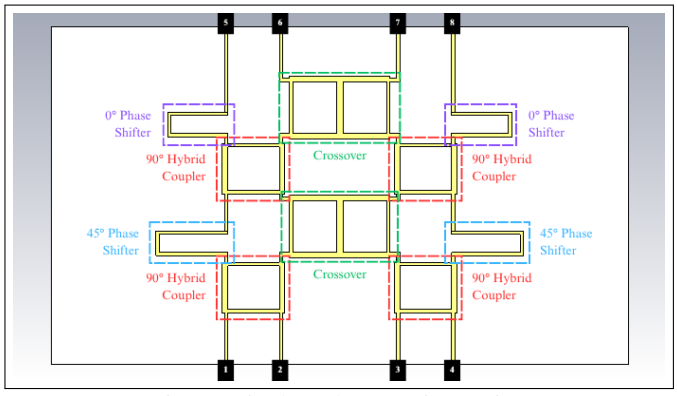

Fig. 1: Final Butler Matrix Design

After assembly and tuning, the final Butler matrix in Figure 1 produced the S-parameter magnitude and phase outputs (S_{X5}, S_{X6}, S_{X7}, S_{X8}) at 900 MHz as presented in Figure 2

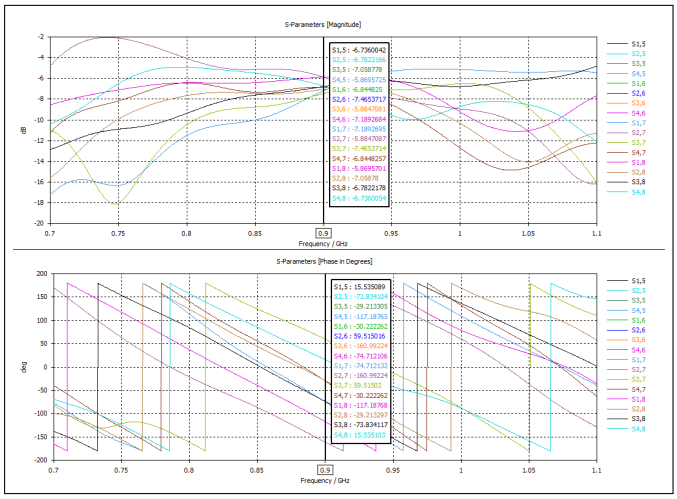

Fig. 2: Butler Matrix S-Parameters (Magnitude & Phase)

TABLE II: Butler Matrix S-Parameter Magnitudes (dB)

MAGNITUDE (dB)				
Output Ports	**Port 1**	**Port 2**	**Port 3**	**Port 4**
S_{X5}	-6.7360042	-6.7822166	-7.0587780	-5.8695725
S_{X6}	-6.8448250	-7.4653717	-5.8847081	-7.1892684
S_{X7}	-7.1892695	-5.8847087	-7.4653714	-6.8448257
S_{X8}	-5.8695701	-7.0587800	-6.7822178	-6.7360054
Imbalance	-1.3196994	-1.5806630	-1.5806633	-1.3196959

TABLE III: Butler Matrix S-Parameter Phases (°)

PHASES (°)				
Output Ports	**Port 1**	**Port 2**	**Port 3**	**Port 4**
S_{X5}	15.535089	-73.834104	-29.213305	-117.187650
S_{X6}	-30.222262	59.515016	-160.992240	-74.712106
S_{X7}	-74.712132	-160.992240	59.515020	-30.222262
S_{X8}	-117.187680	-29.213297	-73.834117	15.535103
$S_{X6} - S_{X5}$	-45.757351	133.349120	-131.778935	42.475544
$S_{X7} - S_{X6}$	-44.489870	139.492744	-139.492740	44.489844
$S_{X8} - S_{X7}$	-42.475548	131.778943	-133.349137	45.757365
Ideal $\Delta\phi$	-45	135	-135	45

and in Tables II and III. Table II shows that Ports 1 and 4 have an imbalance of approximately -1.32 dB, while Ports 2 and 3 have about -1.58 dB — implying symmetry and operates as intended. These imbalances are the result of electromagnetic interference between the microstrips — a phenomenon known as mutual coupling. Although this Butler matrix exhibits imbalance, the focus is on the S-parameter phase outputs since this network relies primarily on steering the beam direction through constructive and destructive interference of the applied phase shifts. Table III shows that the phase differences closely match the ideal values for each port, indicating that the matrix operates as intended and will provide the inputs for the conformal antenna array.

III. Arc Array Factor

To analyze the theoretical behavior of the conformal antenna array, the array factor must be expressed as a function of θ, ϕ, and curvature angle, Φ. As stated by Balanis [9], the array factor shapes the total electric field when multiplied by the single element's field, as shown below:

$$E_{\text{total}} = [\text{Array Factor}] \times [E_{\text{single element at reference point}}] \quad (1)$$

The array factor and total field of an antenna array can be adjusted by varying the element spacing and excitation phase. From the circular array given below:

$$AF(\theta, \phi) = \sum_{n=1}^{N} I_n e^{j[ka\sin(\theta)\cos(\phi - \phi_n) + \alpha_n]}$$

with the radius of the antenna array in this study given as:

$$a = \frac{l_{\text{lin}}}{\Phi} = \frac{3\left(\frac{\lambda_0}{2}\right) + 2\left(\frac{\lambda_0}{4}\right)}{\Phi}$$

where Φ is the parameter of interest that is characterized:

$$\Phi = n\frac{\pi}{4}, \quad n \in \mathbb{Z}, \quad 0 \leq n \leq 4.$$

with the Fraunhofer approximation applied (valid in the far-field, $\theta = 90°$), the arc array factor derived specifically for this study is given as:

$$AF(\phi, \Phi) = \sum_{n=1}^{4} I_n e^{j\left\{\frac{4\pi}{\Phi}\cos\left(\phi - \left[\Phi\left(\frac{2n-1}{8}\right)\right]\right) + \alpha_n\right\}} \quad (2)$$

IV. 4-Element Patch Antenna Array

A. Individual Element

The patch antenna was designed for a 900 MHz center frequency, suitable for rural GSM-900 use [10]. A flexible polyimide substrate ($\epsilon_r = 3.5$) with a height of 1.5 mm was used, meeting the recommended range of $0.003\lambda_0 \leq h \leq 0.05\lambda_0$ for $\lambda_0 = 0.33$ m (free-space wavelength at 900 MHz).

Following Balanis' design method [9], the patch width and actual patch length are:

$$W = \frac{c}{2f_c}\sqrt{\frac{2}{\epsilon_r + 1}} = 111.11\,\text{mm}$$

$$L = \frac{c}{2f_c\sqrt{\epsilon_{\text{eff}}}} - 2\Delta L = 88.82\,\text{mm}$$

The substrate and ground dimensions exceed the patch by $\lambda_0/4$ in length, with the width set as $\lambda_0/2$ to ensure half-wavelength spacing for array integration: $L_s = L_p + \frac{\lambda_0}{4} = 172.15\,\text{mm}$, $W_s = \frac{\lambda_0}{2} = 166.67\,\text{mm}$.

TABLE IV: Dimensions of the Patch Antenna Design

Parameter	Value
Substrate Height	1.5 mm
Patch Length (L_p)	88.82 mm
Patch Width (W_p)	111.11 mm
Substrate/Ground Length (L_s)	172.15 mm
Substrate/Ground Width (W_s)	166.67 mm
Feedline Width	3.39 mm

To ensure that the impedance is matched and provide higher bandwidth and return loss, a well-known impedance matching technique for patch antennas is inset feeding [11]. The inset feed point can be derived from the equation of its input resistance from [9]: $y_0 = \frac{L}{\pi} \cdot \cos^{-1}\left(\sqrt{\frac{R_{in}(y=y_0)}{R_{in}(y=0)}}\right) = 32.26\,\text{mm}$. The component $R_{in}(y = y_0)$ in the derived equation is the characteristic impedance, $Z_0 = 50\,\Omega$, while $R_{in}(y = 0)$ is the resonant input resistance when the antenna is center-fed.

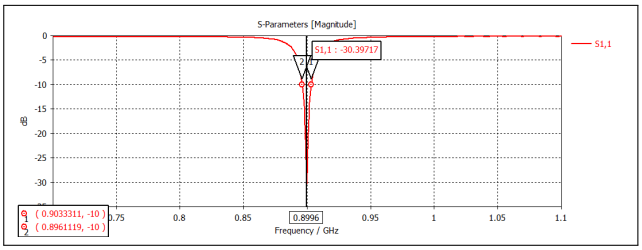

Fig. 3: Minimum S_{11} and -10 dB Bandwidth for $g = 0.678\,\text{mm}$

The inset gap, however, was found by trial-and-error to optimize the patch antenna's S_{11} performance — wherein the best matching occurs at a gap value of $g = \frac{W_{feedline}}{5} = 0.678\,\text{mm}$, with a minimum S_{11} of $-30.3972\,\text{dB}$ and a -10 dB bandwidth of 7219.2 kHz, as shown in Figure 3 — ensuring excellent matching and bandwidth.

B. 4-element Antenna Array Integration

Based on the study in [6], the patch antenna array has elements spaced half a wavelength in free space, measured from the centers of each element.

The expected beam direction can be calculated by $\theta = \sin^{-1}\left(\frac{\lambda_0\Delta\phi}{2\pi d}\right)$, where $\Delta\phi$ is the phase difference between each element of the array, λ_0 is the wavelength in free space, and $d = \frac{\lambda_0}{2}$ is the distance between each element of the array. Table V summarizes the expected phase differences for each port excitation.

TABLE V: Ideal Phases Applied to Each Element for Different Port Excitations

Port Excited	**Port 1** ($-45°$)	**Port 2** ($135°$)	**Port 3** ($-135°$)	**Port 4** ($45°$)
Element 1 Phase (°)	-45	-135	-90	-180
Element 2 Phase (°)	-90	0	-225	-135
Element 3 Phase (°)	-135	-225	0	-90
Element 4 Phase (°)	-180	-90	-135	-45
$\Delta\phi$ (°)	-45	$+135$	-135	$+45$
θ (°)	-14.48	$+48.59$	-48.59	$+14.48$

The inset-tuned patch antenna was integrated into a 4-element array, as shown in Figure 4, with each port fed a magnitude of 0.25 (representing the equal signal division from an input port of the Butler matrix) and phase values defined in Table V. The resulting far-field pattern, presented in Figure 5, serves as a reference for evaluating the chosen conformal antenna.

The curvature was varied using CST's Cylindrical Bend Tool, with radius $a = \frac{l_{\text{lin}}}{\Phi}$, where l_{lin} is the length of the

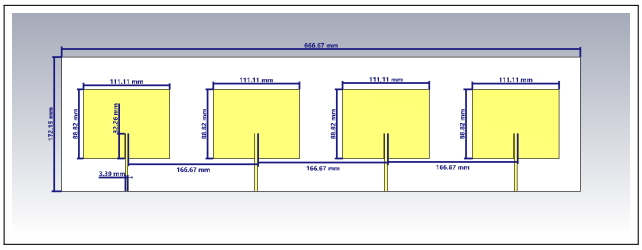

Fig. 4: Linear 4-element Antenna Array

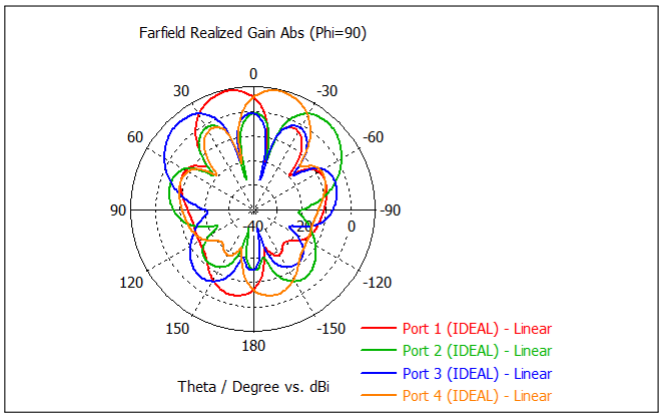

(a) Polar

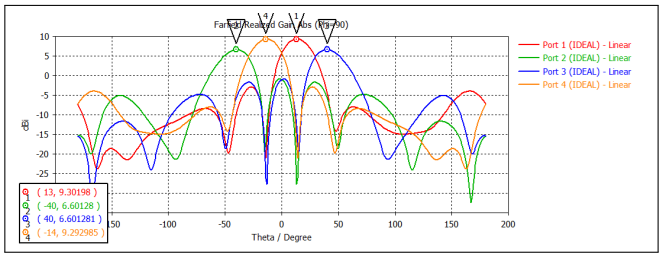

(b) Cartesian

Fig. 5: Linear Antenna Array Farfield Realized Gain Results

antenna array and Φ is the bend angle. Curvatures of $\Phi = \{0°(\text{linear}), 45°, 90°, 135°, 180°\}$, as presented in Figure 6, were tested to evaluate the coverage and angular width, with the optimal case selected for further tuning.

As shown in Figure 7 and Table VI, the $\Phi = 180°$ curvature yields great beam coverage and the widest 3 dB angular widths compared to the other Φ values. However, its gain is insufficient for the intended application — which is due to mutual coupling between the antenna elements caused by the

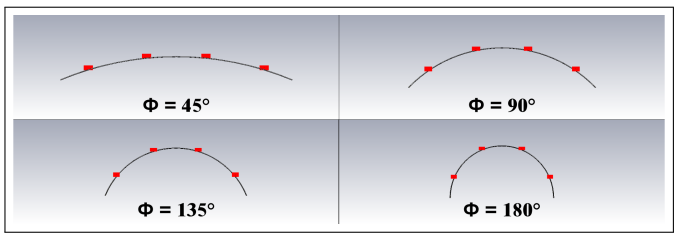

Fig. 6: $\Phi = \{45°, 90°, 135°, 180°\}$ Curvatures (Bottom View)

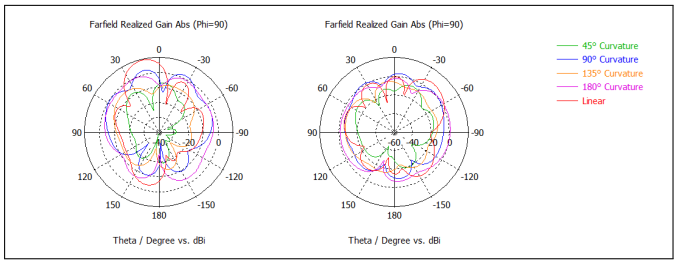

Fig. 7: Farfield Realized Gains for Different Values of Φ for Ports 1 (Left) and 2 (Right)

TABLE VI: Main Lobe Characteristics for Different Curvatures

Curvature	Main Lobe Magnitude (dBi)		Main Lobe Direction (°)		3dB Angular Width (°)	
	Port 1	Port 2	Port 1	Port 2	Port 1	Port 2
Linear	9.3	6.6	13.0	-40.0	25.4	28.0
$\Phi = 45°$	-6.96	-7.43	-7.0	-21.0	22.6	23.5
$\Phi = 90°$	2.42	2.83	14.0	-6.0	21.2	21.5
$\Phi = 135°$	-5.09	-5.29	44.0	8.0	47.4	26.2
$\Phi = 180°$	-0.624	0.987	24.0	-65.0	77.4	72.8

applied curvature — necessitating further tuning to mitigate these effects.

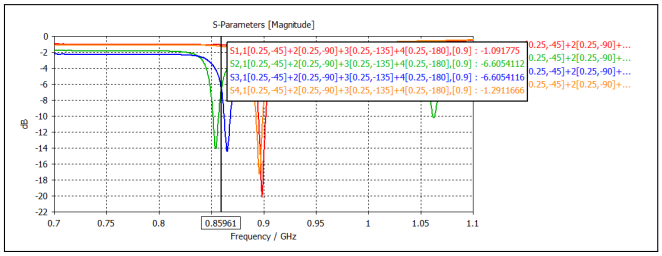

(a) Port 1 Excited

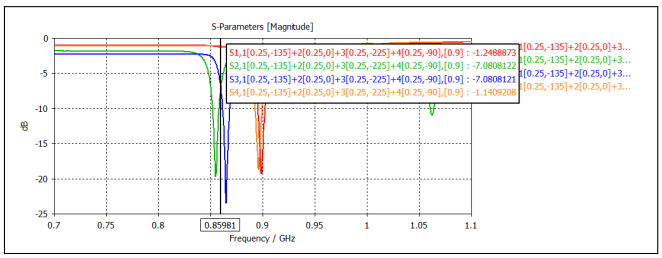

(b) Port 2 Excited

Fig. 8: 180° Curved Antenna Array S-parameters (Pre-tuning)

Figure 8 shows the S-parameters of the $\Phi = 180°$ curved antenna array excited at Ports 1 and 2 with a magnitude of 0.25 and phase values from Table V. Due to mutual coupling, the second and third (central) patches shifted to 0.86 GHz, which is 0.04 GHz below the 900 MHz target. To compensate, these were re-tuned to 920 MHz through iterative adjustments, yielding a recalculated length of 86.88 mm and width of 108.70 mm — obtaining the S-parameters as presented in Figure 9.

Figure 10 presents the dimensions of the final antenna array prior to subjecting to curvature, and Figure 11 presents the final antenna array curved by 180°.

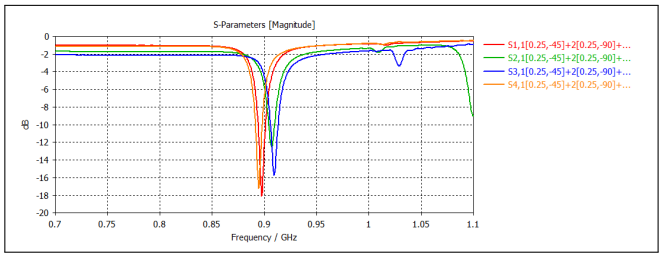

(a) Port 1 Excited

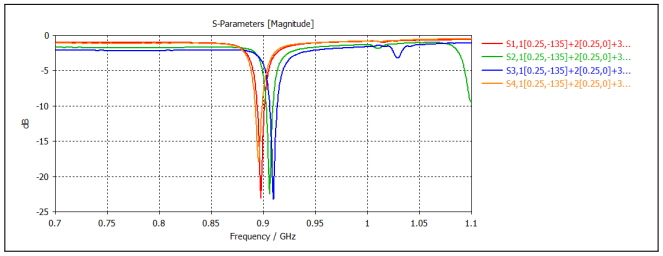

(b) Port 2 Excited

Fig. 9: 180° Curved Antenna Array S-parameters (Post-tuning)

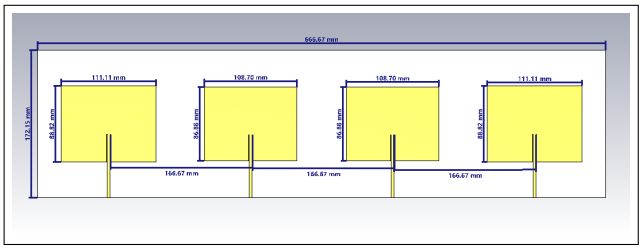

Fig. 10: Pre-curved Final Antenna Array

In order to determine the ideal antenna pattern, the pattern multiplication was obtained based on Equation 1. Figure 12 visually presents the equation (in linear) and Figure 13 presents the plot (in dB) along with the actual results.

TABLE VII: Main Lobe Characteristics for the Linear vs. 180° Curvature

Input Port	Main Lobe Magnitude (dBi)		Main Lobe Direction (°)		3dB Angular Width (°)	
	Linear	$\Phi = 180°$	Linear	$\Phi = 180°$	Linear	$\Phi = 180°$
Port 1	9.3	3.2	13.0	-23.0	25.4	43.4
Port 2	6.6	3.56	-40.0	44.0	28.0	36.0
Port 3	6.6	4.83	40.0	18.0	28.0	33.4
Port 4	9.3	3.36	-13.0	-65.0	25.4	55.9

The actual results of the $\Phi = 180°$ curved antenna array, as

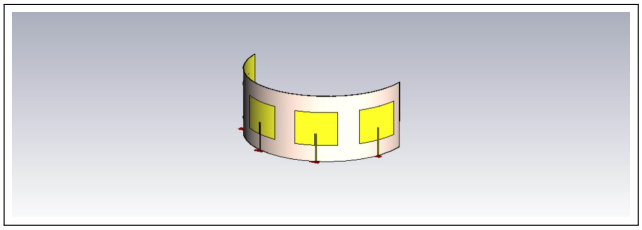

Fig. 11: Final 180° Curved Antenna Array

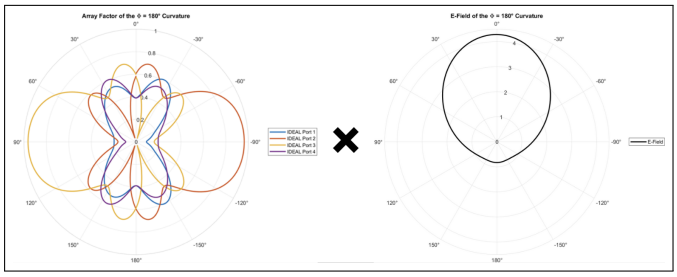

Fig. 12: Pattern Multiplication of the 180° Curvature

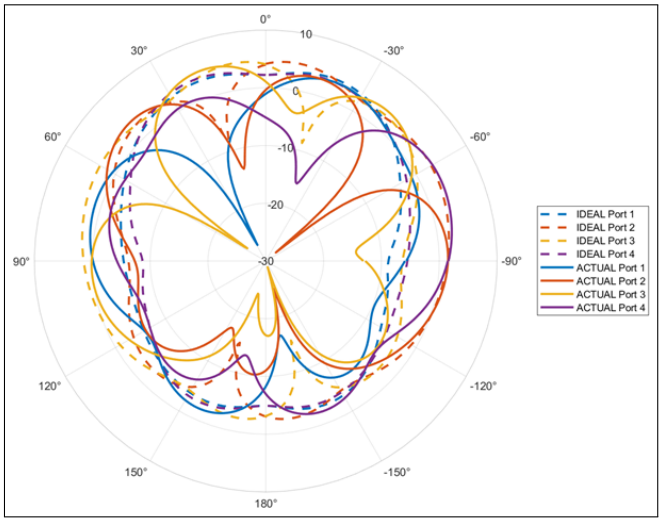

(a) Polar

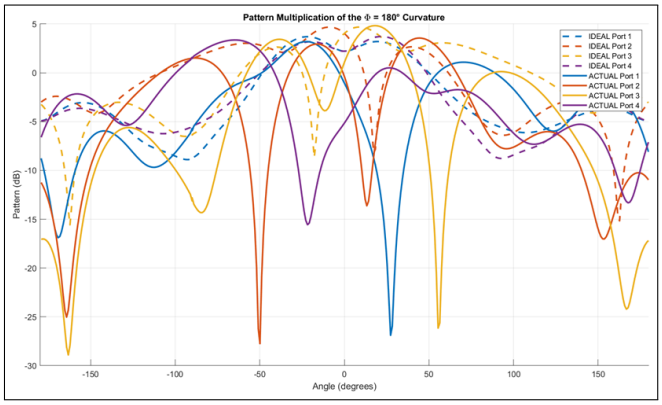

(b) Cartesian

Fig. 13: Pattern Multiplication (Ideal) vs. Butler Matrix-fed (Actual) 180° Curved Antenna Array Gain

presented in Figure 14, compared with the ideal results of the linear antenna array, as presented in Figure 5, are summarized in Table VII.

With this comparison, it is evident that the actual results obtain a wider coverage. However, the main lobe magnitudes are around 2–3 times lower — reasonable since the energy is more spread out. Instead, this output is compared to the pattern multiplication shown in Figure 13 and Table VIII. It also makes sense that the patterns of each port excitation will

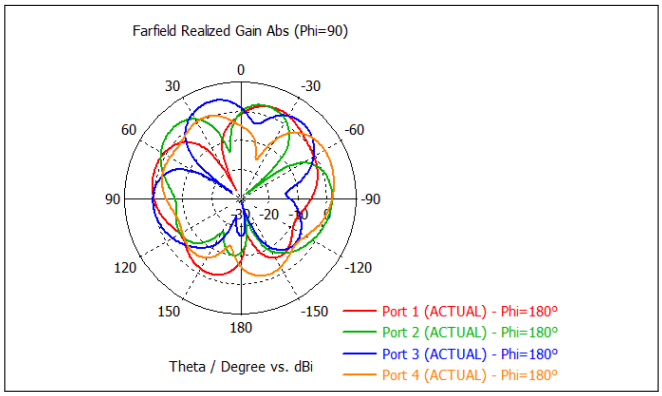

(a) Polar

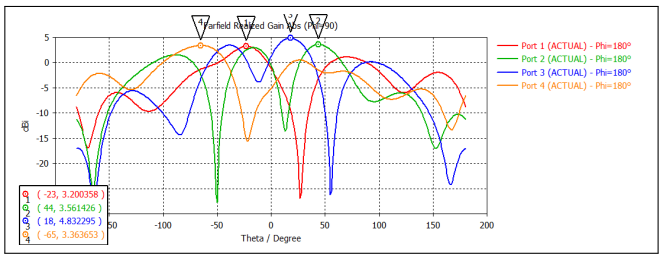

(b) Cartesian

Fig. 14: Butler Matrix-fed 180° Curved Antenna Array

TABLE VIII: Pattern Multiplication (Ideal) vs. Butler Matrix-fed (Actual) 180° Curved Antenna Array Main Lobe Magnitude

Ports	Main Lobe Magnitude (dBi)		Difference (dBi)
	Ideal Output	Actual Output	
Port 1	3.70113	3.2	0.50113
Port 2	4.681	3.56	1.121
Port 3	4.68822	4.83	0.14178
Port 4	3.71996	3.36	0.35996

vary since (1) pattern multiplication ignores coupling effects, and (2) the actual antenna was tuned to compensate for non-idealities.

V. Conclusions

TABLE IX: Curved Antenna Array vs. Pattern Reconfigurable Antenna Main Lobe Magnitude Comparison

$\Phi = 180°$ Curved Antenna Array		Pattern Reconfigurable Inverted-F Antenna [4]	
Direction (°)	Magnitude (dBi)	Direction (°)	Magnitude (dBi)
-23.0	3.2	0	3.5
44.0	3.56	-90	3.0
18.0	4.83	180	4.0
-65.0	3.36	90	1.5

Due to the coverage limitations of [4], which operates only at quadrantal angles in its directional mode as presented in Table IX (relative to its broadside), the Butler matrix-based $\Phi = 180°$ curved antenna array was found most suitable. It provides wider coverage than conventional linear arrays and achieves reasonable gain compared to theoretical pattern multiplication, as shown in Tables VII and VIII. While Port 2 showed the largest deviation of 1.121 dBi, it remains within the acceptable 3–4 dB range of [4]. Despite these positive results, the antenna exhibits trade-offs — one of which is its limited coverage to the front-facing side (0°), with no coverage to the rear (180°). Likewise, the beams resulting from each port excitation are no longer orthogonal, indicating they are no longer spatially distinct, and the realized gains exhibit significant side lobes, wasting power in directions other than where it is needed.

VI. Recommendations

For future work, considering other tuning methods may be done to reduce side lobes, such as probe feeding which involves vertically feeding the patch directly at the $50\,\Omega$ point, and various port excitation combinations may be tested to generate as many radiation patterns as possible and enhance coverage.

References

[1] M. C. Barela *et al.*, "Connecting communities through mobile networks: A case study of implementing community cellular networks in the philippines," in *Introduction to Development Engineering: A Framework with Applications from the Field*, T. Madon, A. J. Gadgil, R. Anderson, L. Casaburi, K. Lee, and A. Rezaee, Eds. Cham: Springer International Publishing, 2023, pp. 567–587, ISBN: 978-3-030-86065-3. DOI: 10.1007/978-3-030-86065-3_21. [Online]. Available: https://doi.org/10.1007/978-3-030-86065-3_21.

[2] A. Weissberger. "The sorry state of 5g sa core networks-smart communications in phillipines." (Oct. 2021), [Online]. Available: https://techblog.comsoc.org/2021/10/04/the-sorry-state-of-5g-sa-core-networks-smart-communications-in-phillipines/.

[3] "The village base station (vbts) project." (2018), [Online]. Available: https://pcarivbts.github.io/.

[4] M. C. L. Purisima, M. Salvador, S. G. P. Agustin, and M. T. Cunanan, "Frequency and pattern reconfigurable antennas for community cellular applications," in *2016 IEEE Region 10 Conference (TENCON)*, 2016, pp. 3767–3770. DOI: 10.1109/TENCON.2016.7848765.

[5] Y. Rahayu and J. R. M. Simanihuruk, "Design of 4x4 butler matrix for beamforming 5g antenna," in *2021 3rd International Conference on Research and Academic Community Services (ICRACOS)*, 2021, pp. 154–159. DOI: 10.1109/ICRACOS53680.2021.9701986.

[6] C.-H. Tseng, C.-J. Chen, and T.-H. Chu, "A low-cost 60-ghz switched-beam patch antenna array with butler matrix network," *IEEE Antennas and Wireless Propagation Letters*, vol. 7, pp. 432–435, 2008. DOI: 10.1109/LAWP.2008.2001849.

[7] K. C. Gupta, R. Garg, I. Bahl, and P. Bhartia, *Microstrip Lines and Slotlines*. Artech House, 1979.

[8] A. B. A. S. Hayat Errifi Abdennaceur Baghdad, "Design and simulation of a planar 4*4 butler matrix in microstrip technology for x band applications," 2017.

[9] C. A. Balanis, *Antenna Theory: Analysis and Design*, Fourth Edition. John Wiley Sons, Inc., 2016.

[10] A. Lodhi, N. Hathi, Y. Gkekas, and P. Nahi, "Coverage comparison of umts networks in 900 and 2100 mhz frequency bands," Feb. 2008, pp. 22 –25, ISBN: 978-0-86341-887-7. DOI: 10.1049/cp:20080136.

[11] J. Singh, "Inset feed microstrip patch antenna," 2017. [Online]. Available: https://api.semanticscholar.org/CorpusID:212524139.